# Confounding factors in multi-parametric q-MRI protocol: A study of bone marrow biomarkers at 1.5 T

Louis Marage, Giulio Gambarota, Jérémy Lasbleiz, Mathieu Lederlin, Hervé Saint-Jalmes

# Confounding factors in multi-parametric q-MRI protocol: a study of bone marrow biomarkers at 1.5 T

Louis Marage [a] *, Giulio Gambarota [a], Jeremy Lasbleiz [a], Mathieu Lederlin [a], Hervé Saint-Jalmes [a].
[a]: Univ Rennes, CHU Rennes, CLCC Eugène Marquis, Inserm, LTSI - UMR 1099, F-35000 Rennes, France.
*Correspondence to: L. Marage, MS, Univ Rennes, LTSI - UMR 1099, 2 Av. du Professeur Léon Bernard, F-35000 Rennes, France.
Mail : louis.marage@univ-rennes1.fr

## ABSTRACT

**Object:** The MRI tissue characterization of vertebral bone marrow includes the measurement of proton density fat fraction (PDFF), $T_1$ and $T_2$* relaxation times of the water and fat components ($T_{1W}$, $T_{1F}$, $T_2^*_W$, $T_2^*_F$), IVIM diffusion D, perfusion fraction f and pseudo-diffusion coefficient D*.
However, the measurement of these vertebral bone marrow biomarkers (VBMBs) is affected with several confounding factors.
In the current study, we investigated these confounding factors including the regional variation taking the example of variation between the anterior and posterior area in lumbar vertebrae, $B_1$ inhomogeneity and the effect of fat suppression on f.

**Materials and Methods:** A fat suppressed diffusion-weighted sequence and two 3D gradient multi-echo sequences were used for the measurements of the seven VBMBs. A turbo flash $B_1$ map sequence was used to estimate $B_1$ inhomogeneities and thus, to correct flip angle for $T_1$ quantification. We introduced a correction to perfusion fraction f measured with fat suppression, namely $f_{PDFF}$.

**Results:** A significant difference in the values of PDFF, f and $f_{PDFF}$, $T_{1F}$, $T_2^*_W$ and D was observed between the anterior and posterior region. Although, little variations of flip angle were observed in this anterior-posterior direction in one vertebra but larger variations were observed in head-feet direction from L1 to L5 vertebrae.

**Discussion:** The regional difference in PDFF, $f_{PDFF}$ and $T_2^*_W$ can be ascribed to differences in the trabecular bone density and vascular network within vertebrae.
The regional variation of VBMBs shows that care should be taken in reproducing the same region-of-interest location along a longitudinal study. The same attention should be taken while measuring f in fatty environment, and measuring $T_1$. Furthermore, the MRI-protocol presented here allows for measurements of seven VBMBs in less than 6 minutes and is of interest for longitudinal studies of bone marrow diseases.

**Keywords**: Quantitative MRI; Bone marrow; Diffusion; IVIM; Relaxometry; Chemical shift imaging.

**Abbreviations**

**PDFF, proton density fat fraction;**

$T_{1W}$**,** $T_1$ **relaxation time of the water;**

$T_{1F}$**,** $T_1$ **relaxation time of the fat**;

$T_2^*{}_W$, $T_2$*** relaxation time of the water**;

$T_2^*{}_F$, $T_2$*** relaxation time of the fat**;

IVIM, IntraVoxel Incoherent Motion;

**f, IVIM perfusion fraction;**

**D, IVIM diffusion coefficient;**

**D*, IVIM pseudo-diffusion coefficient;**

**VBMBs,** vertebral bone marrow biomarkers;

ROI, regions of interest;

RESOLVE, REad-out Segmentation of Long Variable Echo train;

VIBE, Volume Interpolated Breath-hold Examination.

## **1.** INTRODUCTION

In recent years, there have been many advances in the field of MR imaging of bone marrow. Among the different sites of the body where bone marrow resides, the vertebrae have particularly attracted the interest of the MRI scientific community. This is because the vertebral bone marrow is a common site of cancer [1], [2]. Furthermore, pathologies such as osteoporosis induce modifications in the vertebral bone marrow microenvironment and are the cause of vertebral fractures [3], [4]. In general, these tissue microstructural changes -caused by myeloma, osteoporosis or other pathologies- can be detected with $T_1$-, $T_2$- and $T_2$*-weighted MR imaging with significant sensitivity [5]–[10].

In addition to relaxation-weighted imaging, several studies, mainly presented in the recent review by Karampinos et al. [4], have been dedicated to quantify $T_1$, $T_2$ and $T_2$* relaxation times as well as other vertebral bone marrow biomarkers (VBMBs)

such as the proton density fat fraction (PDFF) and the IVIM diffusion and perfusion parameters, namely the diffusion coefficient (D), the pseudo-diffusion coefficient (D*) and the perfusion fraction (f). All these biomarkers are particularly interesting considering myeloma patients follow up [11]–[18]. In addition, since the IVIM perfusion fraction is correlated with enhanced contrast perfusion MRI [1], [14], the use of this biomarker may limit the contrast agents injections.

When quantifying VBMBs, and in general bone marrow biomarkers, an important characteristic of this tissue has to be taken into account. Specifically, the bone marrow differs from other tissues of the human body since it contains two major components (water and fat) that are present in comparable proportions, in addition of trabecular bones. This feature has two main consequences on the assessment of MRI biomarkers such as the relaxation times, the diffusion coefficients and the perfusion fraction. First, for an improved tissue characterization of bone marrow, the separate assessment of the relaxation times of water and fat is necessary [19]–[21]. Secondly, with respect to the quantification of diffusion and perfusion, an efficient fat suppression is necessary to minimize the confounding effects originating from the lipid signal [22]–[24]. But,

this fat suppression bring a confounding effect, this time on the perfusion fraction [24].

In the last few years, a number of studies have been conducted to investigate and tackle the two aforementioned points. First, the separate quantification of the $T_1$ of water ($T_{1W}$), the $T_1$ of fat ($T_{1F}$), the $T_2$* of water ($T_2{}^*_W$), the $T_2$* of fat ($T_2{}^*_F$) and PDFF was achieved using a 3D gradient multi-echo VIBE-Dixon sequence, in two breath-hold acquisitions with two different flip angles [21], [25], [26]. Regarding the second aforementioned point, in a very recent study [24] the effects of the lipid signal and

different fat suppression techniques on the quantification of the IVIM diffusion and perfusion parameters were assessed using the RESOLVE (**re**ad-out **s**egmentation **o**f **l**ong **v**ariable **e**cho train) sequence. In comparison to the single-shot EPI sequence, typically employed in vertebral bone marrow IVIM studies [1], [13], [27]–[32], the RESOLVE sequence allows for the acquisition of images with an improved spatial resolution and reduced distortions [27].

Despite these recent progresses and the growing number of MRI studies on VBMBs quantification, little attention, in general, has been paid to the regional variations of VBMBs within a single vertebra. In particular, little is known regarding 1) the VBMBs spatial heterogeneity in a vertebra and 2) the potential of current quantitative MRI methods to assess, when present, this spatial heterogeneity.

In the current study we sought i) to provide a comprehensive MRI protocol for the measurement of VBMBs and ii) to investigate confounding factors when measuring VBMBs. Two regions of interest, the anterior and posterior area of lumbar vertebrae, were chosen for investigation in young volunteers. Measurements of the PDFF, the relaxation times $T_{1W}$, $T_{1F}$, $T_2{}^*_W$, $T_2{}^*_F$ as well as the IVIM diffusion and perfusion parameters D, D* and f were carried out and the values of VBMBs obtained in the anterior area were compared to those in the posterior area.

## **2.** MATERIALS & METHODS

### *2.1. MR Imaging*

All experiments were conducted on a group of 14 healthy volunteers (7 women and 7 men, age 24 ± 3 years), according to the procedures approved by the local Institutional Review Board, thus informed consent was obtained from all individual

participants included in the study. MRI acquisitions were carried out at 1.5 T (MAGNETOM Aera, Siemens Healthcare, Germany) on the lumbar spine of the volunteers, with the dedicated 32 channels spine coils. The MRI protocol was performed in sagittal orientation and included two sequences: the RESOLVE diffusion-weighted sequence for the measurements of the IVIM parameters and the VIBE-Dixon sequence (3D gradient-echo volumetric interpolated breath-hold examination) acquired at two different flip angles, for the measurements of PDFF, $T_{1W}$, $T_{1F}$, $T_2{}^*_W$ and $T_2{}^*_F$. In order to assess the reproducibility of the technique, for each volunteer, both the VIBE-Dixon and the RESOLVE sequence were performed twice.

The RESOLVE sequence was acquired with the SPAIR (Spectral Attenuated Inversion Recovery) fat suppression module and with the following parameters: TR/TE 2400/58 ms; bandwidth 1330 Hz/Px; FOV 400 x 400 mm²; matrix 188 x 188; 10 slices of 6 mm; iPAT 3; 3 segments in the readout direction; 2 averages; b-values = [0, 50, 100, 150, 400, 800, 1000 s/mm²]. The acquisition time was 4min 41sec.

The VIBE-Dixon sequence was acquired with a TR of 8.2 ms, four echo times: 1.2, 2.4, 4.4 and 6.8 ms, bandwidth 1220 Hz/Px, FOV 325 x 400 mm², matrix 179 x 256, partial fourier 6/8, 72 slices of 4 mm and CAIPIRINHA (Controlled Aliasing In Volumetric parallel imaging results in higher acceleration) total acceleration factor of 4 (2 in phase direction and 2 in slice encoding direction). The VIBE-Dixon acquisition was performed at two flip angles, 5° and 15°, with each acquisition in breath hold lasting 16 seconds. In order to correct the $T_1$ measurements, each VIBE-Dixon was followed by a TurboFLASH $B_1$-Mapping sequence with the following parameters: TR/TE 2000/1.5 ms, flip angles 5° and 15°, bandwidth 490 Hz/Px, FOV 400 x 400 mm², matrix 64 x 64, and 7 slices of 8 mm, for an acquisition time of 4 seconds.

### *2.2. Data Analysis*

Regions-of-interest (ROIs) were drawn in the anterior and posterior region of the five lumbar vertebrae for each volunteer with ImageJ (NIH, Bethesda, MD, http://imagej.nih.gov/ij/). Each ROI had an area of 21 voxels for the images acquired with the RESOLVE sequence, 177 voxels for the VIBE-Dixon. An additional ROI, which included the whole vertebral body, was also drawn to simulate typical ROI analyses performed in previous studies [10], [28], [33], [34].

The original $B_1$ map obtained from TurboFLASH $B_1$-Mapping sequence while assumed to vary smoothly showed some dependence to the underlying tissue characteristics Thus, after a data normalization to the expected flip angle from original $B_1$ map, a morphological mask was applied to remove the unwanted background noise. Afterward, a 3$^{rd}$ order 3D polynomial was fitted to these data, giving a smooth flip angle map (FA-map). This fitting was done with a weighted LinearModelFit function in Mathematica (Wolfram Research, Champaign, IL, USA), the weights being used in order to avoid outliers during the fitting. This method is similar to a published method for a variable flip angle $T_1$-map correction [35].

The values of PDFF, $T_{1W}$, $T_{1F}$, $T_2{}^*_W$ and $T_2{}^*_F$ were obtained by fitting the signal of the multi-echo VIBE-Dixon to a model described in previously published study [20]. In this study, it was shown that 2 angles and 4 echo times was the optimal choice to extract the biomarkers in only two breath holds. For the same reason the fat peak at 5.3 ppm was not taken into account in this study.

The values of $T_{1W}$ and $T_{1F}$ were corrected with the actual flip angles provided by the previously described FA-map.

To extract the IVIM diffusion and perfusion parameters, a two-step segmented algorithm was used [36]. The diffusion coefficient D was first fitted to a mono-exponential function using the 4 higher b-values: 200, 400, 800, 1000 s/mm². In the second step, using all the b-values and the fixed D value obtained in the first step, the IVIM bi-exponential model was used to extract the f and D* values. Considering the 3 components volume model, given in Lasbleiz et al.[37], the PDFF-corrected perfusion fraction $f_{PDFF}$ is given by $f_{PDFF} = f\,(1 - PDFF)$.

Data fitting of both RESOLVE and VIBE-Dixon data was performed using the constrained NonlinearModelFit function in Mathematica.

### *2.3. Statistical analysis*

The values of the VBMBs (PDFF, f, $f_{PDFF}$, $T_{1W}$, $T_{1F}$, $T_2{}^*_W$, $T_2{}^*_F$, D and D*) measured in anterior region were compared to those measured in the posterior region, with the Wilcoxon signed-rank test which is a robust statistical test without *a priori* about the normality of the data distribution. The statistical analysis was performed using the SignedRankTest function in Mathematica. A threshold of $p<0.01$ was used to define statistical significance.

## **3.** RESULTS

Figure 1 (**Fig.1**) shows two MR images (RESOLVE, left and VIBE- Dixon, right) of the spine in one volunteer. The ROIs illustrate the anterior and posterior regions (in cyan and orange color, respectively) that were selected for the data analysis of the VBMBs in each lumbar vertebra. Figure 2 (**Fig.2**) shows two examples of IVIM signal decays of the L3 vertebra, in the same volunteer. One decay corresponds to the L3 anterior region (cyan, squares), the other to the L3 posterior region (orange, triangles). The

bi-exponential fitting curves for the anterior (continuous line) and posterior (dashed line) region are also illustrated. These curves show a good agreement between experimental data and fitted values. A higher perfusion fraction in the posterior region is noticeable when observing the IVIM signal at the b-values between 0 and 200 s/mm². Figure 3 (**Fig.3**) shows the anterior (top graph) and posterior (lower graph) ROI signal, acquired with the multi-echo VIBE-Dixon at 5°(filled circle) and 15° (cross) on the same volunteer. The fitted curves are also displayed; a good agreement between experimental data and fitted values is observed. Visual inspection of these curves suggests a difference between the anterior and posterior region: for instance, when observing the out-phase echoes (2.4 ms and 6.8 ms) the difference in signal between the 5° and 15° is more pronounced in the anterior region, compared to the posterior region.

Table 1 summarizes the result of the data analysis of the VBMBs, showing the mean and standard deviation values calculated over all volunteers, in the anterior and posterior region of the lumbar vertebrae. $R_1$ column indicates the values in the first measurement; and $R_2$ refers to the second one. The p-value from the Wilcoxon signed-rank test is provided in the last column. Those in bold correspond to a p-value less than the significance threshold of 0.01. The $f_{PDFF}$ p-value (~$10^{-4}$ on average) is higher than the f one (~$10^{-5}$ on average). The corrected perfusion fraction $f_{PDFF}$ is smaller than the measured perfusion fraction f value by 30 % and 37 % respectively in anterior and posterior region on average. Two additional tables that compare the measurements in the whole vertebral body and those done in the anterior and the posterior area are available in the Supplementary Material. The differences are significant between the whole area and the anterior one for the five biomarkers from

the double Dixon method. Furthermore, the differences are significant between the whole area and the posterior area for the IVIM parameters and the $f_{PDFF.}$

Figure 4 (**Fig.4**) shows the sagittal FA-map fitted from the overlaid raw data (not colorized), masked and normalized to the native flip angle, at the isocenter slice for a native flip angle of 15°. The plot profiles (white lines) in the head-foot and anterior-posterior, upper (dot) and lower (triangle) plot respectively, are also visible. We can see both the fitted (blue) and the normalized raw (orange) data points which are in good agreement. The tissue related variation of raw data is mainly visible in the anterior-posterior direction, near the $40^{th}$ pixel.

Figure 5 (**Fig.5**) represents an explicative scheme of the corrected perfusion fraction with proton density fat fraction and its interest. We can consider A and B to be two volumes (ROI or voxel) with 3 compartments namely tissue lipids, tissue water and blood perfusion. The numerical values of PDFF are inspired by the study of Carmona et al. [16] from the L4-S2 highly myelotoxic baseline for A and post-treatment for B. In this example, while the two volumes A and B have the same actual perfusion fraction $f_{PDFF}$ = 10 %, the fractions measured with fat suppression, f = 17% (A) or 33% (B), are significantly higher than actual perfusion fraction, but also are significantly different from each other. The perfusion fraction value measured with fat suppression is very sensitive to the fat content in the volume of interest.

## **4.** DISCUSSION

**In the current study, we measured in lumbar vertebral bone marrow of young healthy volunteers the following VBMBs: the proton density fat fraction, the perfusion fraction, the $T_1$ and $T_2$* relaxation**

**times of the water and fat components, the diffusion and the pseudo-diffusion coefficient. The measurement of these VBMBs was performed in the anterior and posterior region of each lumbar vertebra. A significant difference between the anterior and posterior values of proton density fat fraction, perfusion fraction and its corrected version, $T_1$ of fat, $T_2$* of water and diffusion coefficient was observed.**

### *4.1. Proton density fat fraction and perfusion fraction*

**The proton density fat fraction and the perfusion fraction are important biomarkers in clinical and research settings because of their direct physiological interpretation. Among the VBMBs measured in the current study, these two biomarkers display the largest significant difference between anterior and posterior regions. The proton density fat fraction measured in the posterior region was higher than the one measured in the anterior region. This result is in agreement with physiological fact that, in the young population, yellow bone marrow agglomerates more likely around the large vessel in the posterior region of the vertebra. Again, only present in the young population, this fat pattern is very well illustrated in the study of Ricci et al.** [38]**. This known regional**

**differences justify the choice of these two regions for the current study on young healthy volunteers.**

**With respect to the values of proton density fat fraction in vertebrae, the review of Karampinos et al.** [4] **reported values around 30% from several studies, in young volunteers. The vertebral proton density fat fraction measured in the current study is in good agreement with these literature values.**

**The perfusion fraction measured in the posterior region was higher than the one in the anterior region. This result can be readily explained when looking at the anatomical structure of the vertebra, which displays a higher vascularization in the posterior region. The values of the perfusion fraction measured in the current work are in agreement with previous studies performed in young healthy volunteers. Marchand et al.** [28] **measured a perfusion fraction of 14 ± 6 %, in an ROI that included the whole vertebral body; Lasbleiz et al.** [37] **reported a perfusion fraction of 12 ± 3 %, measured in the anterior vertebral region.**

**To our knowledge, the IVIM measurement with fat suppression of perfusion fraction measurement was never corrected. Thus, no literature value comparison is available. Nevertheless, $f_{PDFF}$ is still significantly different between anterior and posterior. We are aware that the correction effect is not important due to the small fat**

**fraction difference (~ 4 %) but this correction becomes mandatory in the case of longitudinal studies with strong PDFF variation as shown in the Carmona et al. study** [16]**.**

### *4.2. $T_2$* relaxation times of water and fat*

**A significant difference was observed in the $T_2$* of water between the anterior and posterior region; specifically, the $T_2$* of water was shorter in the posterior part of the vertebra. It should be noted that a higher trabecular bone density, which induces microscopic magnetic field inhomogeneity, characterizes the posterior region** [39], [40]**. These inhomogeneities are most likely the origin of the observed shortening of the $T_2$* of water in the posterior region. No significant difference was observed in the $T_2$* of fat between the anterior and posterior region, despite the fact that the increased microscopic inhomogeneity should have an effect also on the $T_2$* of fat.**

**The $T_2$* of water measured in the current study is in good agreement with two previous studies** [20], [21] **(13.7 ± 2.9 ms and 12.7± 5.3 ms, in the anterior region), where the same quantification method was applied. Similarly, the $T_2$* of fat are close to the measurements from those two previous studies** [20], [21] **(11.4 ± 2.7ms and 15.9 ± 3.8 ms, in the anterior region).**

### *4.3.T1 relaxation times of water and fat, $B_1$ inhomogeneity*

**The $B_1$ inhomogeneity correction is advisable when using variable flip angle method to calculate $T_1$** [41]**. The $B_1$ variation remains small in the anterior-posterior direction at the short scale of a single vertebra (~1°). On the other hand, this variation is significant through the spine (from 16° at the isocenter to 13° at the lower border of the field of view). The correction must be applied to calculate the mean $T_1$ value of vertebrae or compare vertebra at different locations more accurately.**

**The $T_1$ of water displayed no significant difference between the anterior and posterior region. On the other hand, the $T_1$ of fat was significantly longer in the posterior region. In a previous study, Hu and Nayak** [42] **investigated the $T_1$ of water and fat in phantoms and observed a decrease of the $T_1$ of fat with increased proton density fat fraction. In the current study, we observed a longer $T_1$ of fat in the posterior region, which displays a higher proton density fat fraction (34% vs 30% on average) than the anterior region. There is no clear explanation for these findings. It should be pointed out that our experiment was performed *in vivo* on vertebral bone marrow, which is a tissue more complex than the water-fat phantoms**

**employed by Hu and Nayak. As a matter of fact, the bone marrow includes additional tissue components such as the trabecular bone, which substantially affects the tissue microenvironment.**

**In a previous study** [20]**, where a similar quantification method was used, it was observed a $T_{1W}$ = 701 ± 151 ms and a $T_{1F}$ = 334 ± 113 ms in the anterior region of lumbar vertebrae. These values are slightly different than those observed in the current study. It should be noted that in the current study we performed an additional acquisition, that is, the $B_1$ mapping. The additional information regarding the flip angle was here used to correct the $T_1$ measurement. This newly applied correction could explain the $T_1$ differences between the previous and the current study. Furthermore, $T_1$s values previously measured by Träber et al.** [43] **($T_{1W}$ = 882 ± 33 ms and $T_{1F}$ = 266 ± 2 ms) and Biffar et al.** [44] **($T_{1W}$ = 872 ± 129 ms and $T_{1F}$ = 324 ± 81 ms) in the whole vertebral body and with a different acquisition method are comparable to the values observed in the current study.**

### *4.4. IVIM diffusion and pseudo diffusion coefficients*

**Regarding the other two IVIM parameters, namely D and D*, a robust IVIM fitting method was applied with fixed D method** [36]**.**

**The value of D in the anterior region was significantly smaller than in the posterior region. The magnitude of the difference, however, was small and at this stage, its origin is not clear.**

**With the respect to the D value measured in healthy volunteers in previous IVIM studies, Lasbleiz et al.** [37] **reported a value of 0.42 ± 0.07 × $10^{-3}$ mm²/s, using the RESOLVE sequence with the same b-values as the current study; Marchand et al.** [28] **observed a value of 0.60 ± 0.09 × $10^{-3}$ mm²/s with a single shot EPI sequence and 5 b-values (0, 50, 100, 200, 600 s/mm²). Furthermore, in a literature review by Dietrich et al.** [3] **an average apparent diffusion coefficient of 0.45 ± 0.25 × $10^{-3}$ mm²/s, measured in vertebrae using the mono-exponential model, was reported. Overall, the D value observed in the current study is consistent with the previous IVIM studies and mono exponential measurements.**

**Similarly to the D value, D* was smaller in the anterior region. In one measurement, the difference anterior vs posterior was statistically significant, whereas in other measurement a p-value of 0.01 was observed. With the exception of D*, it should be noted that for all other biomarkers measured in the current study, the first and second measurement yielded consistent results with respect to the statistical comparison between the anterior and posterior region.**

**The values of D* measured in the current study are in good agreement with those observed in previous studies (16 ± 6 × $10^{-3}$ $mm^2/s$, Lasbleiz et al.** [37]**; 28 ± 9 × $10^{-3}$ $mm^2/s$, Marchand et al.** [28]**).**

Lastly, it should be noted that the measurement of regional variations in the IVIM parameters was feasible thanks to the RESOLVE sequence, which allows for a higher spatial resolution when compared to the single shot EPI sequence.

### *4.5. ROI positioning in vertebral bone marrow studies*

**In the current study,** we have investigated regional variations of VBMBs and observed a spatial heterogeneity **between the anterior and posterior regions** in number of biomarkers. In other words, the values of VMBMs change with the ROI positioning.

Furthermore, we observed a significant difference between the values of VMBMs measured in the whole vertebral body and those measured in the anterior and posterior regions. It should be pointed out that quantitative analyses are often performed on ROIs including the whole vertebra volume [10], [28], [33], [34].

**Thus, in longitudinal studies care should be taken in reproducing the same ROI location along the whole study. The approach of choosing the entire vertebral body overcomes this issue of ROI positioning. However, this approach results in an averaging of VBMB values over tissue regions with different characteristics and thus might yield a potential loss of information.**

### *4.6.Short quantitative protocol for vertebral bone marrow studies*

**We have implemented a quantitative protocol to measure in vertebral bone marrow the following biomarkers: the proton density fat fraction, the perfusion fraction, the $T_1$ and $T_2$* relaxation times of the water and fat components, the diffusion and the pseudo-diffusion coefficient. The advantages of this protocol include the short acquisition time (less than 6 minutes) and the use of clinically available MRI sequences. Thus, it can be used for both research studies and diagnostic examinations.**

### *4.7. Limitations*

**This study has numbers of limitations. First, a small number of volunteers was examined. Thus, no investigation of gender specific differences was conducted. Secondly, the $T_2$ relaxation time quantification was not quantified. A more complete protocol would include this biomarker, for a complete characterization of vertebral bone marrow.**

## **5.** CONCLUSION

In the current study, we investigate confounding factors while measuring vertebral bone marrow biomarkers in healthy volunteers. We showed the complementarity of the IVIM perfusion fraction and the proton density fat fraction measurements in fatty

medium. We measured a significant difference in proton density fat fraction, perfusion fraction, $T_1$ of fat, $T_2$* of water and diffusion coefficient between the anterior and posterior region of lumbar vertebrae in young volunteers. **This result highlights** the importance of knowledge of confounding factors in the measurement of biomarkers in bone marrow, and this is even more important in the case of **longitudinal studies.** The quantitative protocol presented in this study takes less than 6 minutes and uses clinically available MRI sequences. Thus, it can be applied in both research and clinical settings.

## **6.** AUTHOR CONTRIBUTIONS

**Louis Marage:** Conceptualization, Methodology, Software, Formal analysis, Investigation, Writing - Original Draft, Visualization.

**Giulio Gambarota:** Conceptualization, Methodology, Validation, Writing - Original Draft, Visualization.

**Jeremy Lasbleiz:** Conceptualization, Validation, Writing - Review & Editing.

**Mathieu Lederlin:** Conceptualization, Writing - Review & Editing, Supervision.

**Hervé Saint-Jalmes:** Conceptualization, Methodology, Software, Validation, Investigation, Writing - Review & Editing, Supervision.

## Acknowledgments

The authors would thank the radiographers and technicians of Rennes University Hospital (Hôpital Sud) for their kind support. The volunteers were included in the OSS-IRM study, supported by the University Hospital of Rennes and the University of Rennes.

Supplementary data

Supplementary material

## REFERENCES

[1] C. Bourillon *et al.*, “Intravoxel Incoherent Motion Diffusion-weighted Imaging of Multiple Myeloma Lesions: Correlation with Whole-Body Dynamic Contrast Agent–enhanced MR Imaging,” *Radiology*, vol. 277, no. 3, pp. 773–783, Dec. 2015, doi: 10.1148/radiol.2015141728.

[2] M. Takasu *et al.*, “Iterative Decomposition of Water and Fat with Echo Asymmetry and Least-Squares Estimation (IDEAL) Magnetic Resonance Imaging as a Biomarker for Symptomatic Multiple Myeloma,” *PLOS ONE*, vol. 10, no. 2, p. e0116842, Feb. 2015, doi: 10.1371/journal.pone.0116842.

[3] O. Dietrich, T. Geith, M. F. Reiser, and A. Baur-Melnyk, “Diffusion imaging of the vertebral bone marrow: DIFFUSION IMAGING OF THE VERTEBRAL BONE MARROW,” *NMR in Biomedicine*, vol. 30, no. 3, p. e3333, Mar. 2017, doi: 10.1002/nbm.3333.

[4] D. C. Karampinos *et al.*, “Quantitative MRI and spectroscopy of bone marrow: Quantitative MR of Bone Marrow,” *Journal of Magnetic Resonance Imaging*, vol. 47, no. 2, pp. 332–353, Feb. 2018, doi: 10.1002/jmri.25769.

[5] M. R. Nouh and A. F. Eid, “Magnetic resonance imaging of the spinal marrow: Basic understanding of the normal marrow pattern and its variant,” *World Journal of Radiology*, vol. 7, no. 12, p. 448, 2015, doi: 10.4329/wjr.v7.i12.448.

[6] A. Baur-Melnyk *et al.*, “Whole-Body MRI Versus Whole-Body MDCT for Staging of Multiple Myeloma,” *American Journal of Roentgenology*, vol. 190, no. 4, pp. 1097–1104, Apr. 2008, doi: 10.2214/AJR.07.2635.

[7] C. P. Shortt *et al.*, “Whole-Body MRI Versus PET in Assessment of Multiple Myeloma Disease Activity,” *American Journal of Roentgenology*, vol. 192, no. 4, pp. 980–986, Apr. 2009, doi: 10.2214/AJR.08.1633.

[8] X.-X. Jiang, Z.-X. Yan, Y.-Y. Song, and W.-L. Zhao, “A pooled analysis of MRI in the detection of bone marrow infiltration in patients with malignant lymphoma,” *Clinical Radiology*, vol. 68, no. 3, pp. e143–e153, Mar. 2013, doi: 10.1016/j.crad.2012.11.002.

[9] A. Latifoltojar *et al.*, “Whole-body MRI quantitative biomarkers are associated significantly with treatment response in patients with newly diagnosed symptomatic multiple myeloma following bortezomib induction,” *Eur Radiol*, vol. 27, no. 12, pp. 5325–5336, Dec. 2017, doi: 10.1007/s00330-017-4907-8.

[10] F. B. Ergen, G. Gulal, A. E. Yildiz, A. Celik, J. Karakaya, and U. Aydingoz, “Fat Fraction Estimation of the Vertebrae in Females Using the T2*-IDEAL Technique in Detection of Reduced Bone Mineralization Level: Comparison With Bone Mineral Densitometry,” *J Comput Assist Tomogr*, vol. 38, no. 2, p. 5, 2014.

[11] C. Messiou *et al.*, “Assessing response of myeloma bone disease with diffusion-weighted MRI,” *BJR*, vol. 85, no. 1020, pp. e1198–e1203, Dec. 2012, doi: 10.1259/bjr/52759767.

[12] B.-B. Chen *et al.*, “Dynamic Contrast-enhanced MR Imaging Measurement of Vertebral Bone Marrow Perfusion May Be Indicator of Outcome of Acute Myeloid Leukemia Patients in Remission,” *Radiology*, vol. 258, no. 3, pp. 821–831, Mar. 2011, doi: 10.1148/radiol.10100995.

[13] J. Niu *et al.*, “Intravoxel incoherent motion diffusion-weighted imaging of bone marrow in patients with acute myeloid leukemia: a pilot study of prognostic value:

IVIM Parameters in Evaluating Prognosis in AML Patients," *Journal of Magnetic Resonance Imaging*, vol. 46, no. 2, pp. 476–482, Aug. 2017, doi: 10.1002/jmri.25600.

[14] C. Lin *et al.*, "Multiple Myeloma Treatment Response Assessment with Whole-Body Dynamic Contrast- enhanced MR Imaging," *MUSCULOSKELETAL IMAGING*, vol. 254, no. 2, p. 11, 2010.

[15] M. Takasu *et al.*, "Iterative Decomposition of Water and Fat with Echo Asymmetry and Least-Squares Estimation (IDEAL) Magnetic Resonance Imaging as a Biomarker for Symptomatic Multiple Myeloma," *PLOS ONE*, vol. 10, no. 2, p. e0116842, Feb. 2015, doi: 10.1371/journal.pone.0116842.

[16] R. Carmona *et al.*, "Fat Composition Changes in Bone Marrow During Chemotherapy and Radiation Therapy," *International Journal of Radiation Oncology*Biology*Physics*, vol. 90, no. 1, pp. 155–163, Sep. 2014, doi: 10.1016/j.ijrobp.2014.05.041.

[17] M. Fenchel, M. Konaktchieva, K. Weisel, S. Kraus, C. D. Claussen, and M. Horger, "Response Assessment in Patients with Multiple Myeloma during Antiangiogenic Therapy using Arterial Spin Labeling and Diffusion-Weighted Imaging," *Academic Radiology*, vol. 17, no. 11, pp. 1326–1333, Nov. 2010, doi: 10.1016/j.acra.2010.08.002.

[18] J. C. Dutoit, E. Claus, F. Offner, L. Noens, J. Delanghe, and K. L. Verstraete, "Combined evaluation of conventional MRI, dynamic contrast-enhanced MRI and diffusion weighted imaging for response evaluation of patients with multiple myeloma," *European Journal of Radiology*, vol. 85, no. 2, pp. 373–382, Feb. 2016, doi: 10.1016/j.ejrad.2015.11.040.

[19] Q. M. Barber and A. Yahya, “Aspects of spinal bone marrow fat to water quantification with magnetic resonance spectroscopy at 3 T,” *Biomed. Phys. Eng. Express*, vol. 1, no. 4, p. 047001, Oct. 2015, doi: 10.1088/2057-1976/1/4/047001.

[20] C. Le Ster, G. Gambarota, J. Lasbleiz, R. Guillin, O. Decaux, and H. Saint-Jalmes, “Breath-hold MR measurements of fat fraction, $T_1$, and $T_2$* of water and fat in vertebral bone marrow: Bone Marrow Fat Fraction, $T_1$ and $T_2$ *,” *Journal of Magnetic Resonance Imaging*, vol. 44, no. 3, pp. 549–555, Sep. 2016, doi: 10.1002/jmri.25205.

[21] C. Le Ster, J. Lasbleiz, S. Kannengiesser, R. Guillin, G. Gambarota, and H. Saint-Jalmes, “A fast method for the quantification of fat fraction and relaxation times: Comparison of five sites of bone marrow,” *Magnetic Resonance Imaging*, vol. 39, pp. 157–161, Jun. 2017, doi: 10.1016/j.mri.2017.03.001.

[22] H. S. Leitão *et al.*, “Fat deposition decreases diffusion parameters at MRI: a study in phantoms and patients with liver steatosis,” *Eur Radiol*, vol. 23, no. 2, pp. 461–467, Feb. 2013, doi: 10.1007/s00330-012-2626-8.

[23] J. Hansmann, D. Hernando, and S. B. Reeder, “Fat confounds the observed apparent diffusion coefficient in patients with hepatic steatosis,” *Magn Reson Med*, vol. 69, no. 2, pp. 545–552, Feb. 2013, doi: 10.1002/mrm.24535.

[24] J. Lasbleiz, C. Le Ster, R. Guillin, H. Saint-Jalmes, and G. Gambarota, “Measurements of Diffusion and Perfusion in Vertebral Bone Marrow Using Intravoxel Incoherent Motion (IVIM) With Multishot, Readout-Segmented (RESOLVE) Echo-Planar Imaging: IVIM-MRI of Bone Marrow With RESOLVE,” *Journal of Magnetic Resonance Imaging*, Sep. 2018, doi: 10.1002/jmri.26270.

[25] M. Bydder *et al.*, “Relaxation effects in the quantification of fat using gradient echo imaging,” *Magnetic Resonance Imaging*, vol. 26, no. 3, pp. 347–359, Apr. 2008, doi: 10.1016/j.mri.2007.08.012.

[26] C. Le Ster, G. Gambarota, J. Lasbleiz, R. Guillin, O. Decaux, and H. Saint-Jalmes, “Breath-hold MR measurements of fat fraction, $T_1$, and $T_2$* of water and fat in vertebral bone marrow: Bone Marrow Fat Fraction, $T_1$ and $T_2$*,” *Journal of Magnetic Resonance Imaging*, vol. 44, no. 3, pp. 549–555, Sep. 2016, doi: 10.1002/jmri.25205.

[27] D. A. Porter and R. M. Heidemann, “High resolution diffusion-weighted imaging using readout-segmented echo-planar imaging, parallel imaging and a two-dimensional navigator-based reacquisition,” *Magnetic Resonance in Medicine*, vol. 62, no. 2, pp. 468–475, Aug. 2009, doi: 10.1002/mrm.22024.

[28] A. J. Marchand *et al.*, “MRI quantification of diffusion and perfusion in bone marrow by intravoxel incoherent motion (IVIM) and non-negative least square (NNLS) analysis,” *Magnetic Resonance Imaging*, vol. 32, no. 9, pp. 1091–1096, Nov. 2014, doi: 10.1016/j.mri.2014.07.009.

[29] J. S. Baik *et al.*, “Differentiation of focal indeterminate marrow abnormalities with multiparametric MRI: MRI for Focal Bone Marrow Abnormalities,” *Journal of Magnetic Resonance Imaging*, vol. 46, no. 1, pp. 49–60, Jul. 2017, doi: 10.1002/jmri.25536.

[30] E. Y. P. Lee *et al.*, “Intravoxel incoherent motion MRI assessment of chemoradiation-induced pelvic bone marrow changes in cervical cancer and correlation with hematological toxicity: IVIM Marrow Changes After Chemoradiation,” *Journal of Magnetic Resonance Imaging*, vol. 46, no. 5, pp. 1491–1498, Nov. 2017, doi: 10.1002/jmri.25680.

[31] S. Park, K.-S. Kwack, N.-S. Chung, J. Hwang, H. Y. Lee, and J. H. Kim, “Intravoxel incoherent motion diffusion-weighted magnetic resonance imaging of focal vertebral bone marrow lesions: initial experience of the differentiation of nodular hyperplastic hematopoietic bone marrow from malignant lesions,” *Skeletal Radiology*, vol. 46, no. 5, pp. 675–683, May 2017, doi: 10.1007/s00256-017-2603-z.

[32] M. A. Yoon, S.-J. Hong, C. H. Lee, C. H. Kang, K.-S. Ahn, and B. H. Kim, “Intravoxel incoherent motion (IVIM) analysis of vertebral bone marrow changes after radiation exposure from diagnostic imaging and interventional procedures,” *Acta Radiologica*, vol. 58, no. 10, pp. 1260–1268, Oct. 2017, doi: 10.1177/0284185116688380.

[33] T. Baum *et al.*, “Anatomical Variation of Age-Related Changes in Vertebral Bone Marrow Composition Using Chemical Shift Encoding-Based Water–Fat Magnetic Resonance Imaging,” *Front. Endocrinol.*, vol. 9, p. 141, Apr. 2018, doi: 10.3389/fendo.2018.00141.

[34] A. Biffar, A. Baur-Melnyk, G. P. Schmidt, M. F. Reiser, and O. Dietrich, “Quantitative Analysis of the Diffusion-Weighted Steady-State Free Precession Signal in Vertebral Bone Marrow Lesions:,” *Investigative Radiology*, vol. 46, no. 10, pp. 601–609, Oct. 2011, doi: 10.1097/RLI.0b013e31821e637d.

[35] J. J. N. van Schie, C. Lavini, L. J. van Vliet, and F. M. Vos, “Feasibility of a fast method for B1-inhomogeneity correction for FSPGR sequences,” *Magnetic Resonance Imaging*, vol. 33, no. 3, pp. 312–318, Apr. 2015, doi: 10.1016/j.mri.2014.10.008.

[36] S. Barbieri, O. F. Donati, J. M. Froehlich, and H. C. Thoeny, “Impact of the calculation algorithm on biexponential fitting of diffusion-weighted MRI in upper abdominal organs: Impact of the Calculation Algorithm on IVIM Parameters in Upper

Abdominal Organs," *Magnetic Resonance in Medicine*, vol. 75, no. 5, pp. 2175–2184, May 2016, doi: 10.1002/mrm.25765.

[37] J. Lasbleiz, C. Le Ster, R. Guillin, H. Saint-Jalmes, and G. Gambarota, "Measurements of Diffusion and Perfusion in Vertebral Bone Marrow Using Intravoxel Incoherent Motion (IVIM) With Multishot, Readout-Segmented (RESOLVE) Echo-Planar Imaging: IVIM-MRI of Bone Marrow With RESOLVE," *Journal of Magnetic Resonance Imaging*, Sep. 2018, doi: 10.1002/jmri.26270.

[38] "Ricci C, Cova M, Zerhouni E et al. Normal Age-related Patterns of Cellular and Fatty Bone Marrow Distribution in the Axial Skeleton: MR Imaging Study. Radiology. 1990;177:83-88. doi:10.1148/radiology.177.1.2399343." .

[39] H. Chen, S. Shoumura, S. Emura, and Y. Bunai, "Regional variations of vertebral trabecular bone microstructure with age and gender," *Osteoporosis International*, vol. 19, no. 10, pp. 1473–1483, Oct. 2008, doi: 10.1007/s00198-008-0593-3.

[40] X. Banse, J. P. Devogelaer, E. Munting, C. Delloye, O. Cornu, and M. Grynpas, "Inhomogeneity of human vertebral cancellous bone: systematic density and structure patterns inside the vertebral body," *Bone*, vol. 28, no. 5, pp. 563–571, May 2001, doi: 10.1016/S8756-3282(01)00425-2.

[41] Evan K. Fram, "Rapid calculation of T1 using variable flip angle gradient refocused imaging." Magnetic Resonance Imaging, 1987, [Online]. Available: https://doi.org/10.1016/0730-725X(87)90021-X.

[42] H. H. Hu and K. S. Nayak, "Change in the proton $T_1$ of fat and water in mixture," *Magnetic Resonance in Medicine*, vol. 63, no. 2, pp. 494–501, Feb. 2010, doi: 10.1002/mrm.22205.

[43] F. Träber *et al.*, “Determination of H relaxation times of water in human bone marrow by fat-suppressed turbo spin echo in comparison to MR spectroscopic methods,” *Journal of Magnetic Resonance Imaging*, vol. 6, no. 3, pp. 541–548, May 1996, doi: 10.1002/jmri.1880060318.

[44] A. Biffar, A. Baur-Melnyk, G. P. Schmidt, M. F. Reiser, and O. Dietrich, “Multiparameter MRI assessment of normal-appearing and diseased vertebral bone marrow,” *European Radiology*, vol. 20, no. 11, pp. 2679–2689, Nov. 2010, doi: 10.1007/s00330-010-1833-4.

*Table 1 Numerical values of VBMBs, expressed as mean ± standard deviation, for both anterior and posterior region for the first and the second repetition (R1, R2 respectively). The p-value from the paired signed rank Wilcoxon test is given for each parameter. * : p-value < 0.01.*

| | **Anterior** | | **Posterior** | | **p-value** | |
|---|---|---|---|---|---|---|
| | **$R_1$** | **$R_2$** | **$R_1$** | **$R_2$** | **$R_1$** | **$R_2$** |
| **PDFF (%)** | 30 ± 10 | 30 ± 8 | 34 ± 10 | 34 ± 10 | **$2.1\ 10^{-6}$ *** | **$2.5\ 10^{-7}$ *** |
| **f (%)** | 14 ± 9 | 16 ± 10 | 22 ± 12 | 21 ± 10 | **$3.2\ 10^{-8}$ *** | **$6.7\ 10^{-4}$ *** |
| **$f_{PDFF}$ (%)** | 10 ± 6 | 11 ± 6 | 14 ± 7 | 13 ± 6 | **$1.5\ 10^{-5}$ *** | **$8.7\ 10^{-3}$ *** |
| **$T_{1W}$ (ms)** | 780 ± 190 | 785 ± 176 | 768 ± 189 | 761 ± 189 | 0.18 | 0.11 |
| **$T_{1F}$ (ms)** | 295 ± 92 | 308 ± 87 | 336 ± 99 | 338 ± 86 | **$2.9\ 10^{-4}$ *** | **$3.8\ 10^{-3}$ *** |
| **$T_2{}^*_W$ (ms)** | 13 ± 4 | 13 ± 4 | 12 ± 5 | 12 ± 4 | **$4.0\ 10^{-3}$ *** | **$8.5\ 10^{-7}$ *** |
| **$T_2{}^*_F$ (ms)** | 13 ± 20 | 10 ± 5 | 11 ± 7 | 12 ± 7 | 0.51 | 0.13 |

| | | | | | | |
|---|---|---|---|---|---|---|
| **D ($\times 10^{-3}$ mm²/s)** | 0.39 ± 0.12 | 0.44 ± 0.26 | 0.42 ± 0.12 | 0.49 ± 0.20 | **2.7 $10^{-3}$ *** | **6.7 $10^{-5}$ *** |
| **D* ($\times 10^{-3}$ mm²/s)** | 18 ± 12 | 18 ± 10 | 23 ± 15 | 26 ± 17 | 0.01 | **4.7 $10^{-4}$ *** |

**Fig.1** Sagittal MR Images of the spine acquired with the RESOLVE sequence (left), b = 0 s/mm², and the DIXON sequence (right), TE = 1.23 ms and FA = 5°, in a healthy volunteer. ROIs are shown with cyan and orange circles for anterior and posterior regions, respectively.

**Fig.2** Signal intensity for the anterior region (cyan square) and posterior region (orange triangle) versus the b-value and the bi-exponential fitting in one same lumbar vertebra (L3). The cyan-continuous line represents the fit for the anterior region (f = 7 %, D = 0.42 × $10^{-3}$ mm²/s, D* = 12 × $10^{-3}$ mm²/s) and the orange-dashed line represents the posterior one (f = 20 %, D = 0.54× $10^{-3}$ mm²/s, D* = 12× $10^{-3}$ mm²/s).

**Fig.3** Signal intensity for the 5° (lighter filled circle) and 15° (darker cross) native flip angle acquisitions versus echo time. The models fitting in one lumbar (L3) vertebra for the anterior (top blue continuous line; PDFF = 31%, $T_{1W}$ = 730 ms, $T_{1F}$ = 256 ms, $T_2{}^*_W$ = 15 ms, $T_2{}^*_F$ = 13 ms) and the posterior region (bottom orange dashed line; PDFF = 37%, $T_{1W}$ = 657 ms, $T_{1F}$ = 382 ms, $T_2{}^*_W$ = 13 ms, $T_2{}^*_F$ = 10 ms) are shown.

**Fig.4** Flip Angle map overlaid by masked original sagittal B1-map. Plot profiles (white lines) show both the fitting (blue) and the raw data (orange), from head to feet direction (upper, dots style) and from left to right direction (lower, triangle style).

**Fig.5** Scheme illustrating the perfusion fraction measurement and its correction $f_{PDFF}$ = f * (1 - PDFF). Let A and B be two volumes of interest. The volumes A and B could model different locations in the same vertebra. Alternatively, the volume A could

model a whole vertebra and the volume B could model 1) a different vertebra from the A vertebra or 2) the vertebra A measured at a different time point, as it is usually done in longitudinal studies. The change in PDFF results in a different value of the observed perfusion fraction; this can be corrected by measuring the PDFF and using the proposed correction factor.

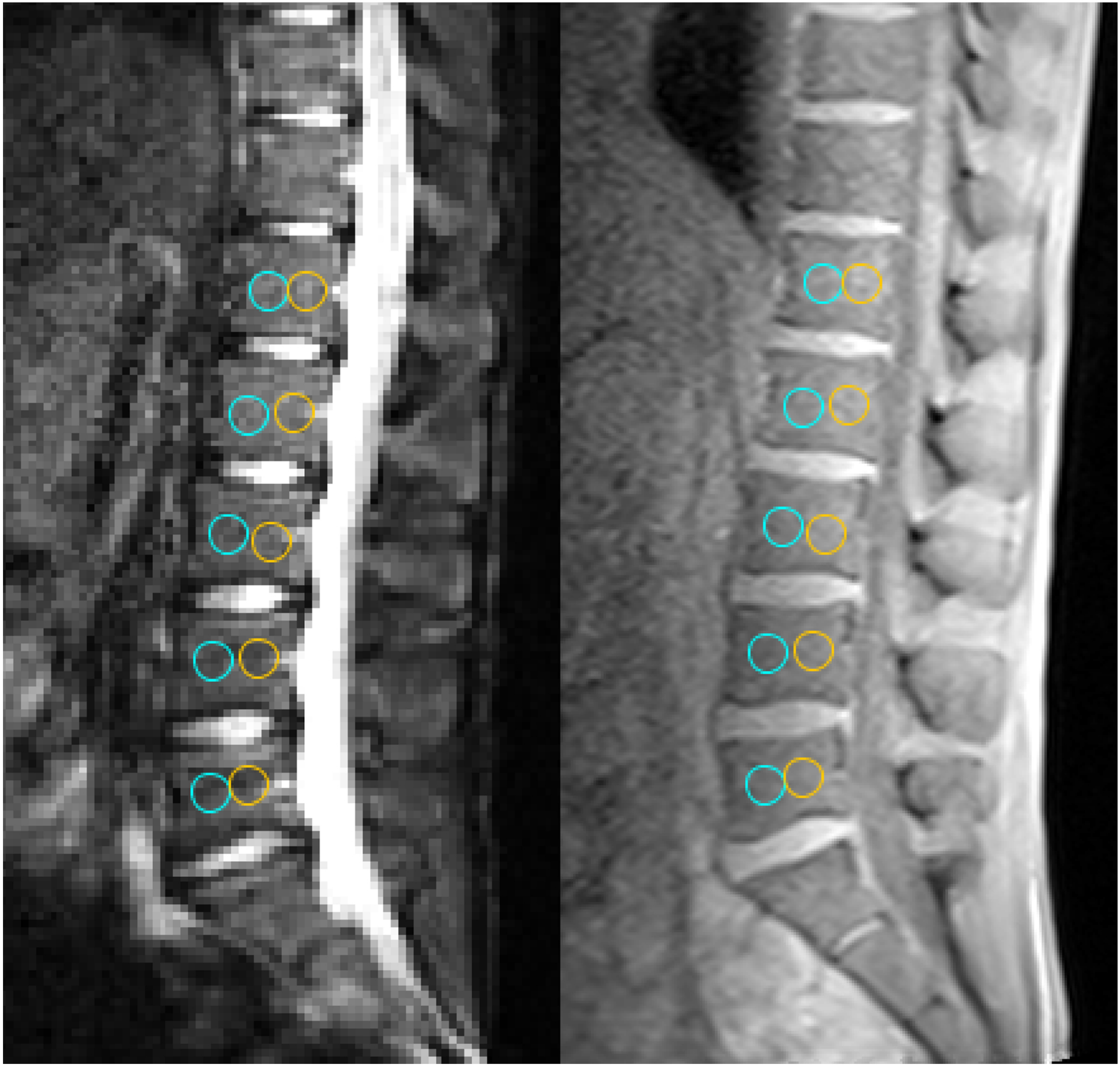

Figure 1

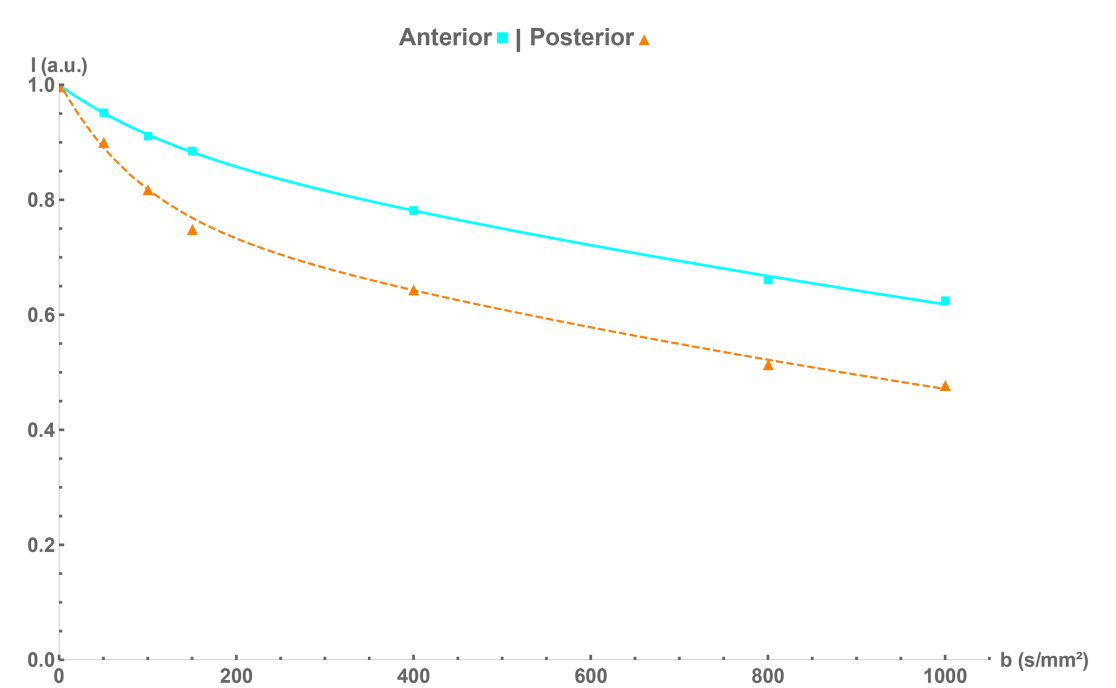
Anterior | Posterior
I (a.u.)
1.0
0.8
0.6
0.4
0.2
0.0
0
200
400
600
800
1000
b (s/mm²)

Figure 2

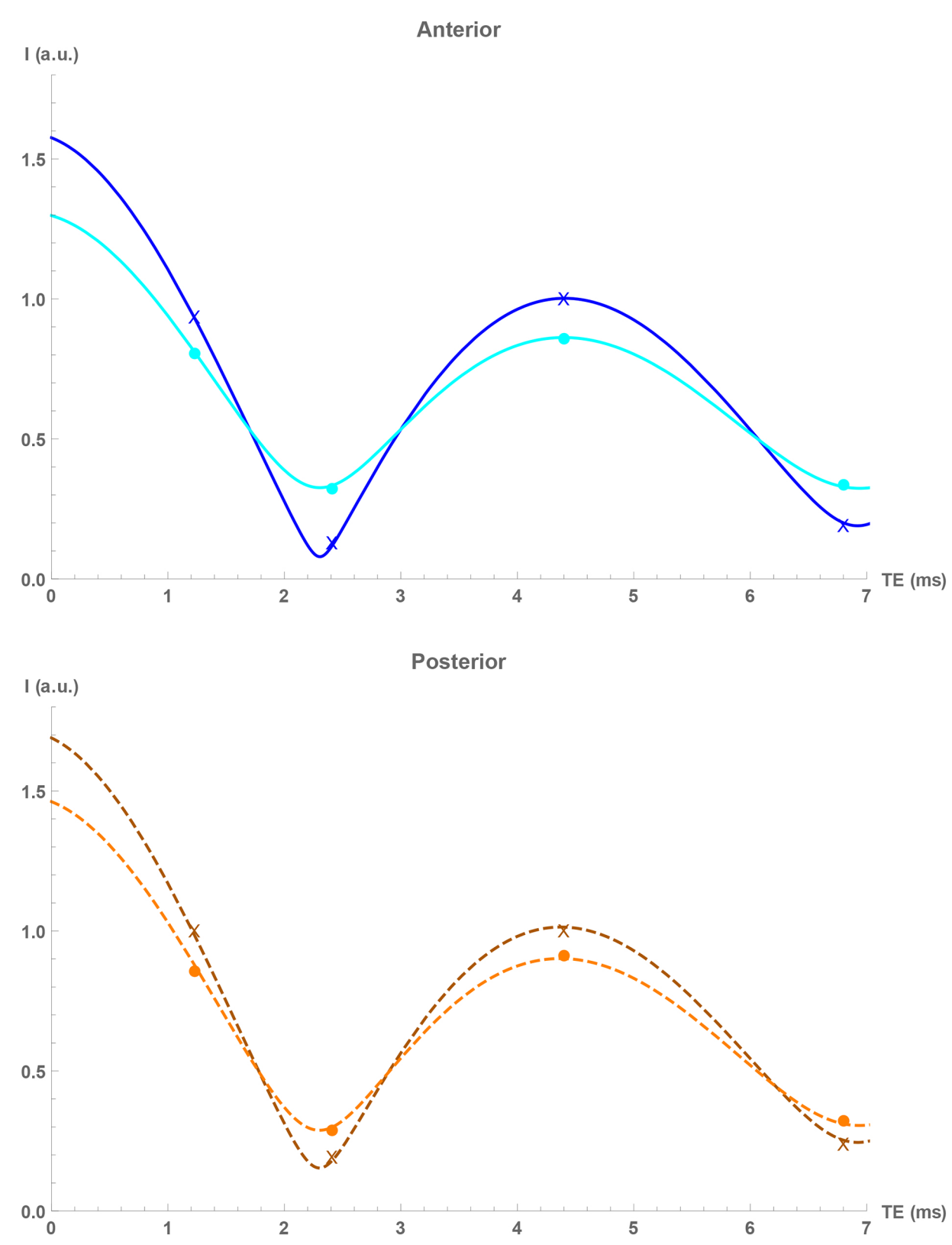
Anterior
I (a.u.)
1.5
1.0
0.5
0.0
0
1
2
3
4
5
6
7
TE (ms)
Posterior
I (a.u.)
1.5
1.0
0.5
0.0
0
1
2
3
4
5
6
7
TE (ms)

Figure 3

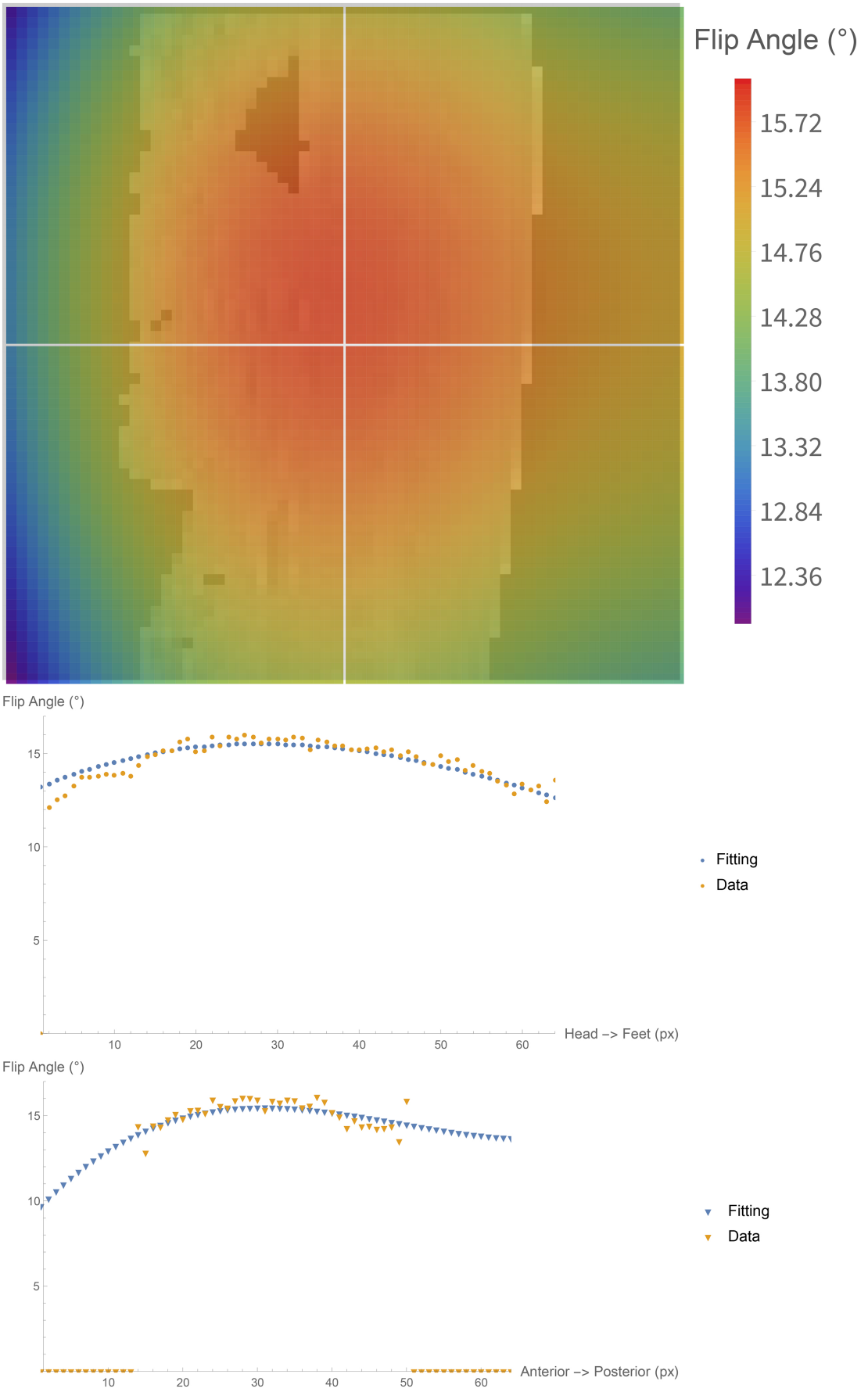
Flip Angle (°)
15.72
15.24
14.76
14.28
13.80
13.32
12.84
12.36
Flip Angle (°)
15
10
5
10
20
30
40
50
60
Head –> Feet (px)
Fitting
Data
Flip Angle (°)
15
10
5
10
20
30
40
50
60
Anterior –> Posterior (px)
Fitting
Data

Figure 4

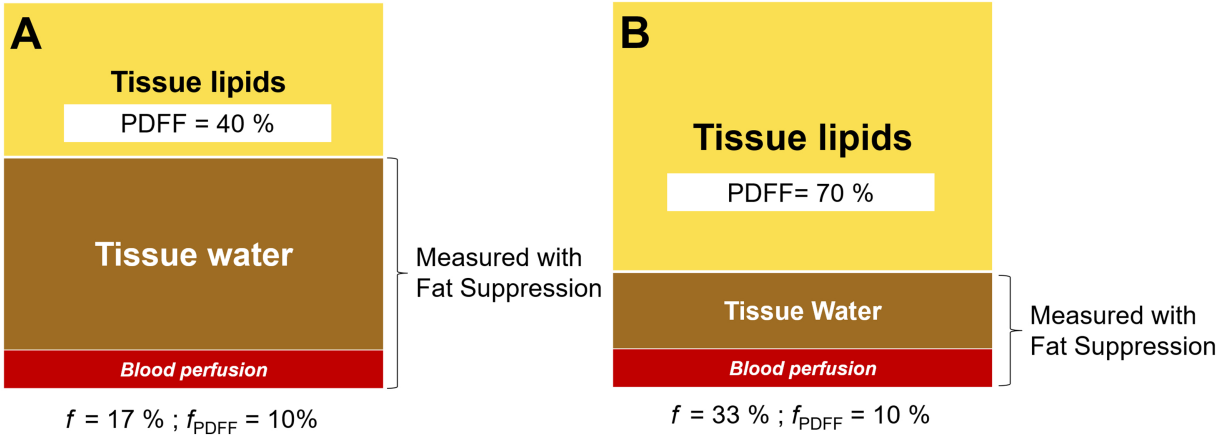
A
Tissue lipids
PDFF = 40 %
Tissue water
Blood perfusion
Measured with
Fat Suppression
f = 17 % ; f_PDFF = 10%
B
Tissue lipids
PDFF= 70 %
Tissue Water
Blood perfusion
Measured with
Fat Suppression
f = 33 % ; f_PDFF = 10 %

Figure 5